Rare Metal Materials and Engineering
Volume 55, Issue 9, September 2026
Available online at www.rmme.ac.cn

Science Press

Cite this article as: Hou Junhan, Yan Zhenzhen, Huang Huang, et al. Structural Origin of Enhanced Stability of Ni-Nb Ultrastable Metallic Glass[J]. Rare Metal Materials and Engineering, 2026, 55(09): 2188-2193. DOI: https://doi.org/10.12442/j.issn.1002-185X.20250487.

ARTICLE

Structural Origin of Enhanced Stability of Ni-Nb Ultrastable Metallic Glass

Hou Junhan, Yan Zhenzhen, Huang Huang, Zhou Jiong, Zhu Fan

College of Smart Materials and Future Energy, Fudan University, Shanghai 200438, China

Abstract: Molecular dynamics simulations were used to simulate the vapor deposition process for the investigation of the structural evolution of Ni-Nb metallic glasses as a function of substrate temperature. Results show that optimal substrate temperature is approximately 850 K, at which the glass attains the lowest potential energy and thus the highest stability. The formation of ultrastable glass is accompanied by a transition of short-range ordered structure from a distorted icosahedron to a perfect icosahedron. This phenomenon can be further confirmed in Mg-Cu-Y, La-Ni-Al, Zr-Cu-Al, and Cu-Zr metallic glass systems. In this research, the structural origin of ultrastable metallic glass formation is established, providing new insights into the nature of the glass transition.

Key words: metallic glass; ultrastable glass; molecular dynamics simulation

1 Introduction

Ultrastable glass has rapidly become a focal point in materials science and condensed matter physics due to its exceptionally high thermal stability and superior mechanical properties[1–5]. Its emergence also presents new opportunities for the investigation of ideal glasses[6]. Ultrastable glass was firstly prepared through physical vapor deposition (PVD) of organic molecules[7]. Since then, the method has been widely applied to various glass systems[8–10], and ultrastable glasses have been used in a broad range of organic materials[10] and metallic systems[11–14]. Particularly, metallic glasses have attracted considerable attention as model glass formers, because of their relatively simple atomic structures and well-defined thermodynamic characteristics. For instance, Yu[15] and Aji[16] et al achieved ultrastable zirconium-based glasses via magnetron sputtering deposition at $0.7T_g - 0.8T_g$, where T_g indicates the glass transition temperature. Similarly, Wang et al[13] demonstrated that gold-based metallic glasses deposited at $0.70T_g - 0.95T_g$ exhibit higher crystallization activation energies than melt-spun ribbon samples. Magagnosc et al[17] further analyzed the palladium-based metallic glasses and found that deposition within the $0.7T_g - 0.8T_g$ window yields samples with enhanced hardness. In addition, Zhao et al[18] reported that cerium-based metallic glasses aged at room temperature (about $0.85T_g$) for more than 17 years evolve into ultrastable glasses with exceptional resistance against crystallization.

A common explanation for the formation of ultrastable glasses is the markedly enhanced molecular mobility at the surface of amorphous materials relative to their bulk counterparts[19]. This enhanced mobility enables deposited atoms to rearrange into denser configurations, thereby lowering the system energy. Paeng et al[20] measured the surface influence depth in polystyrene and found that the thickness of the mobile surface layer is increased with the increase in temperature. Chen et al[21] compared surface and bulk diffusion rates in several small-molecule glasses and observed that near the glass transition temperature, the surface diffusion rate of indomethacin exceeds the bulk diffusion rate by approximately six orders of magnitude. For metallic glasses, the surface diffusion is five orders of magnitude faster than the bulk diffusion[22]. Despite these perspectives, direct evidence linking the enhanced surface mobility with the formation of ultrastable glasses is rare, which is largely due to the difficulty of probing dynamic processes using conventional experimental techniques. As a result, molecular

Received date: September 22, 2025
Foundation item: National Natural Science Foundation of China (U23A20606, 52371151); Shanghai Pujiang Program (21PJ1401800)
Corresponding author: Zhu Fan, Ph. D., Associate Professor, College of Smart Materials and Future Energy, Fudan University, Shanghai 200438, P. R. China, Tel: 0086-21-3124-3538, E-mail: fzhu@fudan.edu.cn

dynamics (MD) simulations have been widely used. For example, Reid et al[23] demonstrated that in a 2D glass-forming liquid, vapor-deposited films evolve from highly square-grid features to locally ordered pentagonal arrangements as the film stabilizes. Leoni et al[24] used vapor deposition simulations of a model glass former and found that the content of stable locally-optimal icosahedral structures reach the maximum value at optimal deposition temperatures. Those structures exhibited microscopic features similar to those of well-aged glasses.

Substrate temperature is a critical parameter in the deposition process, and experimental studies have demonstrated its strong influence on the resultant glass properties[25–26]. Ultrastable glasses are typically formed within the temperature range of $0.70T_g - 0.95T_g$, which is a specific optimal window closely related to the kinetic characteristics of the glass transition. The results in Ref. [27] suggested that the surface dynamics governing ultrastable glass formation is primarily controlled by β-relaxation processes. In this study, MD simulations were employed to investigate the structural evolution of as-deposited $Ni_{62}Nb_{38}$ metallic glasses at various substrate temperatures. Building on these results, the established mode of structural evolution was applied to Mg-Cu-Y, La-Ni-Al, Zr-Cu-Al, and Cu-Zr systems[28–30], elucidating the structural origin underlying the formation of ultrastable metallic glasses.

2 Methods

2.1 Simulation procedure for deposition process

LAMMPS molecular dynamics package was used to construct a $Ni_{62}Nb_{38}$ (at%) metallic glass via PVD. Interatomic interactions were described using the embedded-atom method[31]. The substrate consisted of 1600 silicon atoms arranged in a diamond lattice with an exposed (001) crystal plane. Interactions among silicon atoms were described by the modified Tersoff potential[32], whereas interactions between the deposited Ni-Nb atoms and the silicon substrate were modeled using a weak Lennard-Jones potential[33] with ε=0.2 eV and σ= 0.32 nm (ε and σ are related model parameters), ensuring that the substrate served solely as a mechanical support for the growing film.

During deposition, the substrate temperature was maintained at 750–900 K. Vapor-phase atoms were introduced randomly at a sufficiently large height above the substrate along the z-direction (perpendicular to the substrate surface) with the initial velocities corresponding to those at kinetic temperature of 2000 K. The atomic trajectories were propagated under NVE ensemble. The deposition rate was approximately 0.45 m/s, and the total deposition duration was 8 ns. After deposition, PVD film was relaxed for 3 ns, and 30 configurations were extracted during the final 1 ns of relaxing for subsequent structure and property analyses.

2.2 Calculation and analysis of simulation results

The internal structure of the as-deposited glass was obtained by firstly removing the substrate and then performing energy minimization while keeping the simulation box dimensions fixed. Based on the strong influence of surfaces on atomic energy and local structure, the atoms located within the central region of the film were used for analysis of the as-deposited metallic glass. The thickness was approximately 2.0 nm. The average atomic potential energy of the system was calculated by weighting the mean potential energies of Ni and Nb atoms according to their atomic fraction (62:38).

The radial distribution function (RDF) $g(r)$ can be calculated by Eq.(1), as follows:

$$g(r) = \frac{V}{\rho N}\left[\sum_{i=1}^{N}\sum_{j\neq i}\delta\left(r - r_{ij}\right)\right] \quad (1)$$

where V is the system volume, ρ is the number density, N is the total number of atoms, r_{ij} is the distance between atoms i and j, and $\delta(r-r_{ij})$ is the Dirac delta function accounting for atomic pairs at distance r. The local bond-orientational order parameters were calculated using the definitions mentioned in the following part. The complex function $q_{lm}(i)$ for atom i is defined by Eq.(2)[34], as follows:

$$q_{lm}(i) = \frac{1}{N_b(i)}\sum_{j=1}^{N_b(i)} Y_{lm}\left(r_{ij}\right) \quad (2)$$

where $N_b(i)$ is the number of nearest neighbors of atom i; l is an integer; m runs from $-l$ to $+l$; $Y_{lm}(r_{ij})$ is the spherical harmonic function evaluated for the function r_{ij} from atom i to atom j. The average bond-orientational order parameter is then given by Eq.(3)[35], as follows:

$$\bar{q}_{lm}(i) = \frac{1}{\tilde{N}_b(i)}\sum_{j=1}^{\tilde{N}_b(i)} q_{lm}(k) \quad (3)$$

where the definitions of all terms in Eq. (3) are described in Ref. [35]. Finally, the average local bond-orientational order parameter is calculated by Eq.(4)[35], as follows:

$$Q_l(i) = \sqrt{\frac{4\pi}{2l+1}\sum_{m=-l}^{l}\left|\bar{q}_{lm}(i)\right|^2} \quad (4)$$

where the definitions of all terms in Eq. (4) are described in Ref. [35]. Usually, the parameters Q_4 and Q_6 are used to distinguish crystalline from amorphous structures.

3 Results and Discussion

3.1 Microstructure of as-deposited Ni-Nb film

MD simulations were conducted to analyze deposition models at substrate temperatures of 750, 800, 825, 850, 875, and 900 K. Fig. 1a presents the schematic diagram of the deposition model. Fig. 1b and 1c show RDFs and atomic potential energies, respectively.

As shown in Fig. 1b, the height of the first RDF peak varies with the substrate temperature, indicating that the substrate temperature modulates the degree of short-range order in the deposited film. Notably, the peak height reaches its maximum at 850 K, suggesting that the most ordered local arrangements for Ni and Nb atoms can be achieved at this temperature. Besides, the position of the first peak also exhibits negligible changes, implying that the average bond length remains nearly constant.

Similarly, the average atomic potential energy displays a

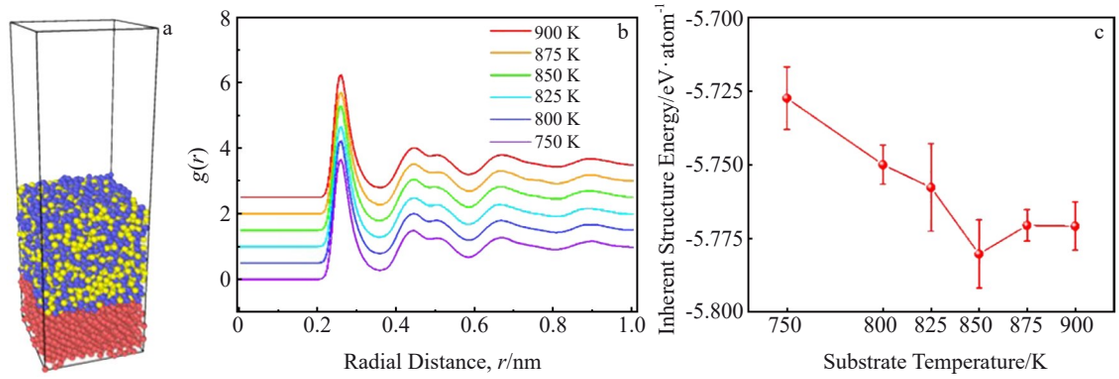

Fig.1 Schematic diagram of as-deposited glass film on Si substrate (a); RDFs $g(r)$ at different substrate temperatures (b); inherent structure energy of as-deposited films at different substrate temperatures (c)

pronounced dependence on the substrate temperature, as shown in Fig. 1c. Under different temperatures (750–900 K), the average potential energy reaches its minimum value at 850 K, indicating that atoms can achieve more stable packing configurations at this temperature, thus lowering the overall system energy. Notably, the temperature of 850 K corresponds to approximately $0.8T_g$ of this system, highlighting it as the optimal temperature for energy-structure co-optimization. This result is in agreement with RDF results.

Fig. 2 shows the bond-orientational order distributions characterized by parameters Q_4 and Q_6. The color bar in Fig. 2 represents the normalized local density of the particle, indicating values from 0 (blue, low density) to 1 (yellow, high density). Characteristic values for perfect body-centered cubic (bcc), face-centered cubic (fcc), and hexagonal close-packed (hcp) crystal structures are marked for reference. The red dashed curve separates ordered and disordered regions. The results are compared with those of bcc, fcc, and hcp structures. Under different temperatures (750–900 K), the Q_4 and Q_6 points are broadly dispersed without dense clusters or sharp distributions in the regions corresponding to crystalline phases, such as fcc, bcc, or hcp phases. This dispersion indicates the absence of long-range order and confirms that the amorphous structure is retained across the temperature range of $0.70T_g$–$0.85T_g$.

To further investigate the evolution of local atomic structures, Voronoi polyhedral analysis was employed to quantify atomic clusters centered on Ni and Nb atoms. Fig. 3a

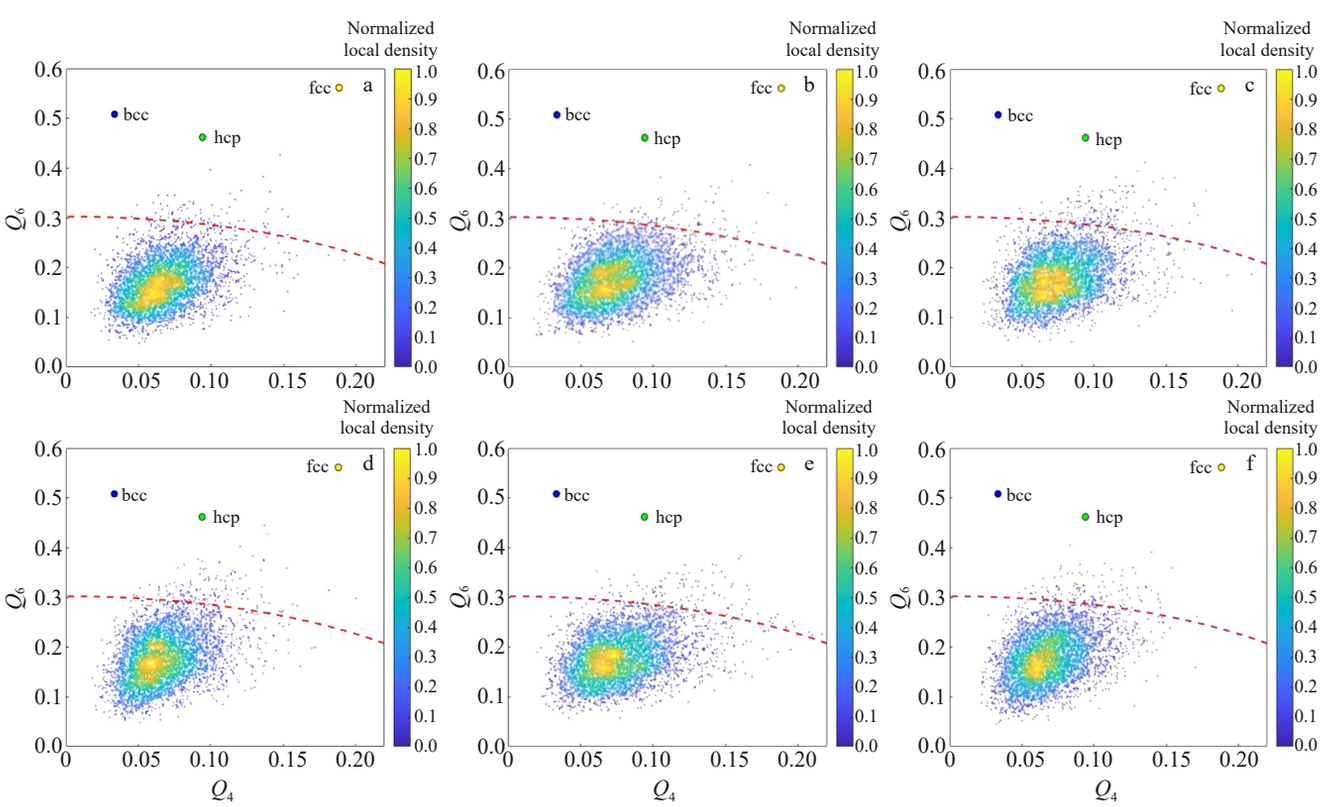

Fig.2 Distributions of bond-orientational order parameters Q_4 and Q_6 at various substrate temperatures: (a) 750 K, (b) 800 K, (c) 825 K, (d) 850 K, (e) 875 K, and (f) 900 K

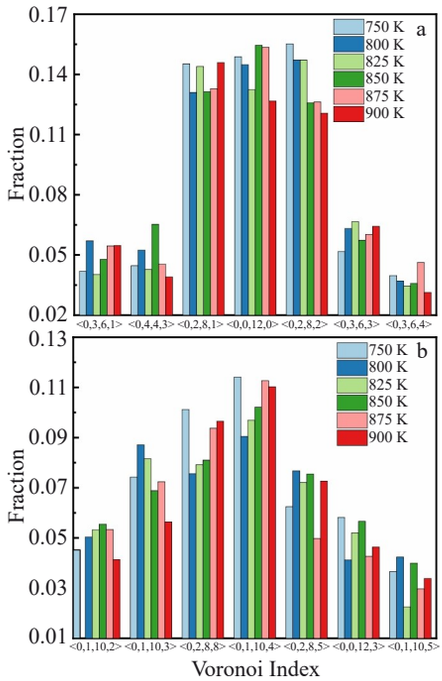

Fig.3 Fraction of the most common Voronoi indices for Ni-centered (a) and Nb-centered (b) atomic clusters at different temperatures

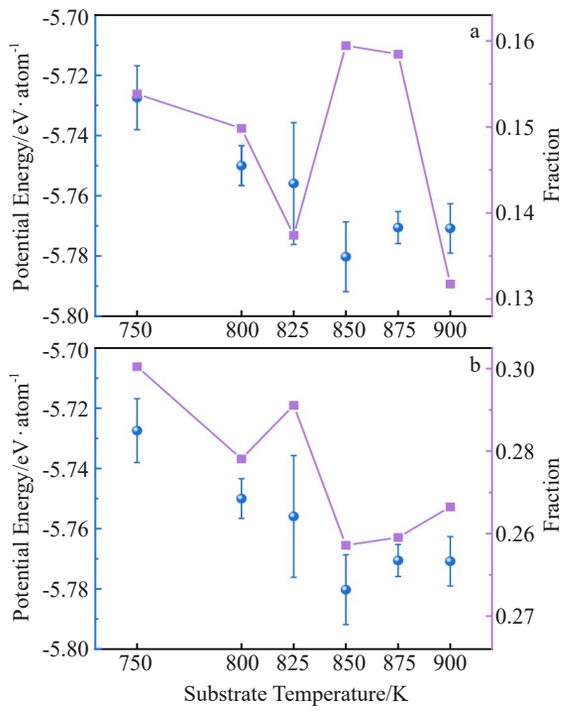

Fig.4 Correlation between potential energy and temperature for different Voronoi indices: (a) icosahedral structures (<0, 0, 12, 0>) and (b) distorted icosahedral structures (<0, 2, 8, 2>, <0, 2, 8, 1>)

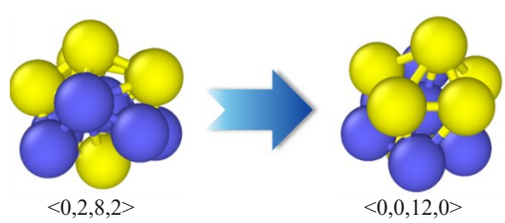

Fig.5 Schematic diagram of structural evolution from distorted icosahedron <0,2,8,2> to full icosahedron <0,0,12,0>

shows the distribution of Voronoi indices for Ni-centered atomic clusters at various temperatures. Ni-centered Voronoi polyhedra primarily form icosahedral structures (<0, 0, 12, 0>) and distorted icosahedral structures (<0, 2, 8, 2>, <0, 2, 8, 1>), while Nb-centered polyhedra tend to adopt high-coordination structures (coordination number≥14), such as <0, 1, 10, 4>. As shown in Fig. 3a, the proportion of the icosahedral structure <0, 0, 12, 0> at 850 K is significantly higher than that at other temperatures, indicating that regular icosahedral configurations are favored at this temperature, whereas both higher and lower temperatures suppress their formation.

To elucidate the driving mechanism of temperature-induced structural evolution, the atomic potential energy was correlated with the populations of icosahedral structures (<0, 0, 12, 0>) and icosahedral-like structures (<0, 2, 8, 2>, <0, 2, 8, 1>). As shown in Fig.4a, the minimum potential energy coincides with the highest proportion of <0, 0, 12, 0> icosahedral structures at 850 K, demonstrating a clear negative correlation between icosahedral ordering and system energy.

Fig. 4b shows that the total fraction of icosahedral-like structures reaches its lowest value at the same optimal temperature. Deviations under these temperatures lead to a noticeable increase in distorted motifs. Combining Fig.4a, the results indicate that near 850 K, a portion of the distorted icosahedral-like clusters are transformed into more stable icosahedral configurations, thereby reducing the system energy and enhancing icosahedral order.

Fig. 5 further illustrates the structural evolution from icosahedral-like structures to fully icosahedral ones. Particularly, the atoms located at quadrilateral or hexagonal vertices of <0, 2, 8, 2> polyhedra rearrange to form pentagonal vertices, eliminating distortions. Combined with the potential energy analysis, this geometric reorganization is not random. Instead, it is intensified with the increase in deposition temperatures and peaks near $0.8T_g$.

3.2 Optimal substrate temperatures for different metallic glasses

Deposition simulations were also performed for $Mg_{65}Cu_{25}Y_{10}$, $La_{50}Ni_{15}Al_{35}$, $Zr_{50}Cu_{40}Al_{10}$, and $Cu_{50}Zr_{50}$ metallic glasses[28–30] at various substrate temperatures, and their inherent structure energies were calculated, as shown in Fig. 6. All systems exhibit minimum potential energies at substrate temperatures below T_g, indicating that each composition reaches an optimal stability temperature, as summarized in Table 1.

Fig. 7 shows the correlation between $0.8T_g$ and optimal substrate temperature for all systems. The T_s values are close to the $0.8T_g$ values, demonstrating that the enhanced stability near $0.8T_g$ is a universal feature across different metallic glasses. At this temperature, α-relaxation (large-scale atomic migration) is substantially suppressed, while β-relaxation (localized rearrangements) is enhanced. This balance prevents

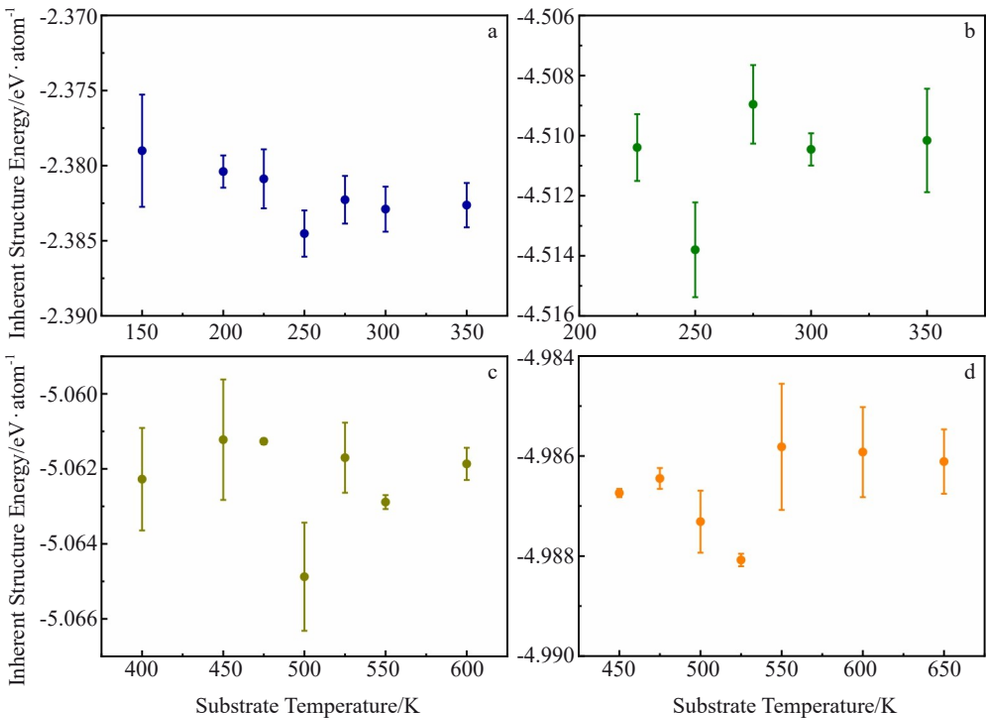

Fig.6 Inherent structure energy of different as-deposited films as a function of substrate temperature: (a) $Mg_{65}Cu_{25}Y_{10}$; (b) $La_{50}Ni_{15}Al_{35}$; (c) $Zr_{50}Cu_{40}Al_{10}$; (d) $Cu_{50}Zr_{50}$

Table 1 Optimal substrate temperature (T_s) and glass transition temperature (T_g) of different metallic glasses

Alloy/at%	Optimal substrate temperature, T_s/K	Glass transition temperature, T_g/K	T_s/T_g
$Mg_{65}Cu_{25}Y_{10}$	250	411	0.61
$La_{50}Ni_{15}Al_{35}$	250	470.3	0.53
$Zr_{50}Cu_{40}Al_{10}$	500	685	0.73
$Cu_{50}Zr_{50}$	525	695	0.76
$Ni_{62}Nb_{38}$	850	945	0.90

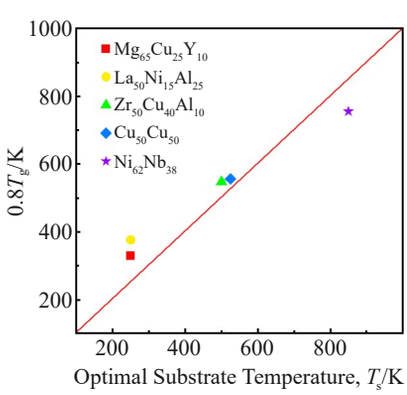

Fig.7 Correlation between $0.8T_g$ and optimal substrate temperature of different metallic glass systems

excessive disorder at high temperatures and structural freezing at low temperatures, thereby facilitating the formation of ultrastable glasses.

4 Conclusions

1) $Ni_{62}Nb_{38}$ films deposited at substrate temperature of $0.8T_g$ exhibit significantly lower atomic potential energy compared to the films deposited at other substrate temperatures, indicating a minimum potential energy and optimal thermodynamic stability. Furthermore, deposition at $0.8T_g$ facilitates the transformation of icosahedral-like structures into ideal icosahedral configurations, thereby enhancing short-range order and overall structural stability.

2) The optimal substrate temperature is approximately $0.8T_g$ for several metallic glass systems, suggesting a universal behavior. At this temperature, large-scale atomic migration (α-relaxation) is suppressed, whereas localized rearrangement (β-relaxation) is enhanced. This balance prevents excessive disorder at high temperatures and structural freezing at low temperatures, facilitating the formation of ultrastable glasses.

References

1 Ediger M D. *The Journal of Chemical Physics*[J], 2017, 147(21): 210901
2 Debenedetti P G, Stillinger F H. *Nature*[J], 2001, 410(6825): 259
3 Rodríguez-Tinoco C, González-Silveira M, Ramos M A *et al*. *Rivista del Nuovo Cimento*[J], 2022, 45: 325
4 Luo P, Fakhraai Z. *Annual Review of Physical Chemistry*[J], 2023, 74: 361
5 Ngai K L. *Progress in Materials Science*[J], 2023, 139: 101130
6 Yu H B, Yang Q. *Acta Physica Sinica*[J], 2017, 66: 176108
7 Swallen S F, Kearns K L, Mapes M K *et al*. *Science*[J], 2007,

315(5810): 353
8 Luo P, Wolf S E, Govind S *et al*. *Nature Materials*[J], 2024, 23: 688
9 Walters D M, Antony L, de Pablo J J *et al*. *The Journal of Physical Chemistry Letters*[J], 2017, 8: 3380
10 Guo Y L, Morozov A, Schneider D *et al*. *Nature Materials*[J], 2012, 11: 337
11 Liu S Y, Cao Q P, Wang X D *et al*. *Thin Solid Films*[J], 2016, 616: 608
12 Liu M, Cao C R, Lu Y M *et al*. *Applied Physics Letters*[J], 2017, 110: 031901
13 Wang J Q, Chen N, Liu P *et al*. *Acta Materialia*[J], 2014, 79: 30
14 Chen N, Frank R, Asao N *et al*. *Acta Materialia*[J], 2011, 59: 6433
15 Yu H B, Luo Y, Samwer K. *Advanced Materials*[J], 2013, 25: 5904
16 Aji D P B, Hirata A, Zhu F *et al*. *ArXiv Condensed Matter: Materials Science*[J], 2013: 1306.1575
17 Magagnosc D J, Feng G, Yu L *et al*. *APL Materials*[J], 2016, 4: 086104
18 Zhao Y, Shang B S, Zhang B *et al*. *Science Advances*[J], 2022, 8(33): eabn3623
19 Ediger M D, Forrest J A. *Macromolecules*[J], 2014, 47: 471
20 Paeng K, Ediger M D. *Macromolecules*[J], 2011, 44: 7034
21 Chen Y, Zhang W, Yu L. *The Journal of Physical Chemistry B*[J], 2016, 120: 8007
22 Cao C R, Lu Y M, Bai H Y *et al*. *Applied Physics Letters*[J], 2015, 107: 141606
23 Reid D R, Lyubimov I, Ediger M D *et al*. *Nature Communications*[J], 2016, 7: 13062
24 Leoni F, Martelli F, Royall C P *et al*. *Physical Review Letters*[J], 2023, 130: 198201
25 Chua Y Z, Ahrenberg M, Tylinski M *et al*. *The Journal of Chemical Physics*[J], 2015, 142: 054506
26 Ngai K L, Wang L M, Yu H B. *The Journal of Physical Chemistry Letters*[J], 2017, 8: 2739
27 Yu H B, Wang W H, Bai H Y *et al*. *National Science Review*[J], 2014, 1: 429
28 Cheng Y Q, Ma E, Sheng H W. *Physical Review Letters*[J], 2009, 102: 245501
29 Sheng H W, Cheng Y Q, Lee P L *et al. Acta Materialia*[J], 2008, 56(20): 6264
30 Ding J H, Cheng Y Q, Ma E. *Acta Materialia*[J], 2013, 61: 3130
31 Zhang Y, Ashcraft R, Mendelev M I *et al*. *The Journal of Chemical Physics*[J], 2016, 145: 204505
32 Purja P G P, Mishin Y. *Physical Review B*[J], 2017, 95: 224103
33 Zhen S, Davies G J. *Physica Status Solidi A*[J], 1983, 78(2): 595
34 Steinhardt P, Nelson D R, Ronchetti M. *Physical Review B*[J], 1983, 28: 784
35 Wolfgang L, Christoph D. *The Journal of Chemical Physics*[J], 2008, 129(11): 1

超稳 Ni-Nb 金属玻璃稳定性增强的结构起源

侯钧瀚，严珍珍，黄　煌，周　炯，朱　凡
(复旦大学 智能材料与未来能源创新学院，上海 200438)

摘　要：采用模拟气相沉积过程的分子动力学方法，探究Ni-Nb金属玻璃结构随基底温度的演化规律。结果表明：约850 K为最佳基底温度，此时玻璃体系势能最低，稳定性最高。超稳定玻璃的形成伴随着短程有序结构由扭曲二十面体转变为完美二十面体结构。该现象在Mg-Cu-Y、La-Ni-Al、Zr-Cu-Al及Cu-Zr金属玻璃体系中得到进一步验证。本研究明确了超稳定金属玻璃形成的结构起源，可为理解玻璃转变本质提供新视角。

关键词：金属玻璃；超稳玻璃；分子动力学模拟

作者简介：侯钧瀚，男，2002年生，硕士，复旦大学智能材料与未来能源创新学院，上海 200438，E-mail：23210300041@m.fudan.edu.cn